E. Zappa, R. Liu, L. Trainelli, A. Rolando, P. Cordisco, M. Terraneo, M. Redaelli
A Vision-Based Technique for In-Flight Measurement of Helicopter Blade Motion
Experimental Techniques, Vol. 44, N. 1, 2020, p. 1-18
doi:10.1007/s40799-019-00331-1

A vision-based technique for in-flight measurement of helicopter blade motion

E. Zappa[1], R. Liu[1*], L. Trainelli[2], A. Rolando[2], P. Cordisco[3], M. Terraneo[3], M. Redaelli[4]

[1]Department of Mechanical Engineering, Politecnico di Milano, Milan, Italy

[2]Department of Aerospace Science and Technology, Politecnico di Milano, Milan, Italy

[3]Vicoter, Calolziocorte, Italy

[4]Leonardo Helicopters, Cascina Costa di Samarate, Italy

Abstract

The measurement of helicopter main rotor blade angles during flight is a key capability to implement advanced applications, such as strategies for the reduction of emitted noise and to develop innovative flight control laws. The approach proposed in this work for the real-time estimation of blade angles is based on a stereoscopic system mounted on the top of the main rotor and pointing to an optical target placed on the blade root. An advanced image-processing algorithm was developed to match the target features in the left and right camera images, which was required for the 3D reconstruction of the target based on a triangulation method. This algorithm was customized for the target used in this specific application, in order to implement a procedure that is both reliable in blob matching and characterized by a very low computation effort. This allowed the system to speeding up the triangulation procedure aimed at obtaining the 3-D coordinates of the features, in view of real-time applications, even with very compact processing units that can be accommodated on the main rotor head. An inverse problem for the 3-D rotation of the target was solved using the Singular Value Decomposition technique, thus improving the robustness of the measurement. The stereoscopic system was developed in order to be integrated on board an AW139 helicopter main rotor hub, equipped with a synchronous lighting device and a pre-processing unit. The latter enabled the system to automatically extract the

* Corresponding author: rui.liu@polimi.it
Address: Via Giuseppe La Masa, 1, 20156 Milano
Fax: +039 02 2399 8585

minimum set of information to be transferred, by means of a slipring, to the processing unit hosted in the fuselage. For the full assessment of the reliability and accuracy of the integrated system, harsh dynamic and accuracy trials were conducted on laboratory test benches. The harsh dynamic tests demonstrated that the system can work continuously in realistic conditions without any structural or data acquisition problems. The accuracy tests, based on a robot test rig simulating the motion of the blade, demonstrated the capability of the system and the accuracy of the measurement technique developed. The discrepancy between the reference blade angles and the estimated ones was found to be less than 0.36^0 for all the realistic blade angle combinations tested.

Keyword: stereo camera; integrated measurement system on AW139 helicopter; advanced blob matching algorithm; accuracy test; harsh dynamic test

1 Introduction

The capability to gather direct measurements of helicopter rotor blade motion during flight represents a key enabler for multiple advanced applications in rotorcraft technology. As helicopter main and tail rotors are responsible for the generation of the fundamental forces and moments for vehicle vertical lift and steering, the behavior of the rotor blades is strongly related to the rotorcraft performance, stability and control characteristics (see e.g. [1]). The availability of a rotor state measurement system capable of acquiring real-time, reliable data on 3-D blade motion may open the way towards innovative improvements in rotorcraft system design and verification at large, if applied to experimental vehicles, as well as rotorcraft operations, health and usage monitoring applications, and safety and control system augmentations [2], if installed on production aircraft. Moreover, real time rotor state measurement is fundamental for the early prediction of the blade–vortex interaction (BVI), which in turn, is of paramount importance for new generation helicopter design, strongly aiming at reducing both maintenance costs and noise levels [3]. The application of rotor state measurement systems is of great interest also for many other applications, such as the implementation of operator assisting system techniques [4] and the development and validation of control models for tilt-rotor aircrafts [5-6]. To date, the development of rotor state measurement systems has been limited to a few experimental applications, either in laboratory tests or on board instrumented prototypes, and no such systems are available on production rotorcraft.

A survey of available literature shows that only a few papers on vision-based measurement systems for helicopter blade motion estimation are present. However, most of them discuss laboratory or wind tunnel testing. In [7], a blade tracking technique based on a single camera system was applied for the vibration of the blade by using image processing. In [8], a single camera system successfully measured the helicopter blade angles in laboratory testing, while the applicability of vision-based techniques to rotor dynamics analysis is widely explored in literature (see for example [9] and [10]). A stereo imaging system based on 3D image correlation was applied for the full-field displacement of rotary blades in [11] and [12]. However, the uncertainty of digital image correlation (DIC) results is affected by the experimental conditions [13] and in particular by the motion blur that can arise in dynamic applications [14] and [15]. A multi-camera system was developed to measure the blade root motion in pitch, flap and lag over the full azimuthal range for wind tunnel applications in [16]. Concerning on board testing, the only relevant example seems to be the early contribution found in [17], where a single photographic camera was rigidly mounted on the main rotor hub of a Sikorsky HNS-1 helicopter pointing to the blade tip to acquire blade images during flight and post-process them after flight to derive blade angle values.

The present contribution concerns a system recently designed and developed for real-time acquisition of the full blade motion relative to the helicopter for in-flight applications. This capability is considered not only in relation to flight testing activities using dedicated vehicles, be they occasional or routinely performed, but also in view of a possible future production system to be integrated on board existing and future rotorcraft at large. This clearly aims to take into due account considerations on the ability of the measurement system to be produced, integrated, and certified for application on board a rotary-wing vehicle, with the further requirement to be as much as possible portable, i.e. capable to fit different vehicles without changes in the fundamental system architecture and operating mode.

Indeed, this challenging task originated by the request contained in the EU-funded Clean Sky program, under the call JTI-CS-2013-01-GRC-05-008. The MANOEUVRES project [18-19] was launched in 2013 in response to this call, including the design and development of a novel contactless rotor state measurement system. Such a system was required as a fundamental component within a complex framework aimed to allow real-time in-flight monitoring of the noise emission by the rotorcraft pilot. This is intended as an important aid in performing optimal noise-abatement procedures, especially in terminal phases when flying in ground proximity over inhabited or other noise-sensitive areas. This ambitious goal was sought by making use of sophisticated aeroacoustics prediction techniques ([20-21])

which, when combined with the blade flapping measurements provided by the new main rotor state sensor and the equally new Pilot Acoustic Indicator (PAI), i.e. a dedicated cockpit instrumentation [22-23], allow the estimation and pilot presentation of the current emitted noise level. Also, research on Rotor State Feedback (RSF) innovative control laws, enabled by the rotor flapping measurement system, fell within the scope of the MANOEUVRES project [24-25]. At the very basis of this multidisciplinary effort lies the design, implementation and testing of a contactless rotor flapping measurement system. Contactless measuring solutions are targeted in this work because of their expected higher reliability and endurance compared to contact-based measurement systems [26-28]. Moreover, contactless solutions are intrinsically easier to be adapted to different rotor types, providing higher value for a solution designed for a large class of vehicles, not only for future developments, but also for current production rotorcraft.

In this work, we are concerned with the activities carried out in the MANOEUVRES WP2 “Flapping measurement system preliminary studies”. In particular, we build upon a preceding phase involving requirement definition, technology selection, and conceptual design of three candidate solutions, followed by preliminary implementation and testing of such solutions. This process was briefly outlined in [29-30], while a discussion of the candidate measurement systems (based on 2-D laser, single camera, and twin cameras) is given in [31], together with their experimental validation and competitive selection based on accuracy performance. As a result, a measuring solution was chosen for the final measurement system development implementation, in view of a fully-operational flight demonstration. In this work, we focus on the selected measuring solution prototype and describe the detailed study of the requirements and installation constraints for the target helicopter, namely a Leonardo Helicopters AW139 instrumented prototype.

The present paper focuses on the complete development of the selected solution that led to a mature implementation, fully compliant with requirements related to on board integration and qualification for flight. With respect to the laboratory prototype described in [29-30], here we present in due detail the results obtained in a comprehensive experimental campaign performed on the ready-to-fly assembly composed of a stereo camera, a lighting device, a triggering equipment, and the data storage and processing equipment, all installed on a AW139 main rotor head. These results eventually provided evidence needed for obtaining the permit to fly for the instrumented AW139 equipped with the novel rotor state measurement system. As described in Sections 5 and 6, the fully developed measuring system was extensively qualified by means of both harsh dynamic tests and accuracy tests. Harsh dynamic tests mainly focus on the mechanical behavior of the system in terms of modal tests, vibration tests, rotation tests and sunlight sensitivity

tests. These aimed at verifying the robustness of the developed measuring system in realistic conditions. Accuracy tests focused on the evaluation of measurement uncertainty: through the use of a robot arm, a target identical to the one mounted on the real blade was displaced in front of the measuring system, simulating the real blade angles and allowing the measuring system validation.

2 System requirements and preliminary studies

In view of an optimal solution, a preliminary study was carried out in close cooperation with Leonardo Helicopters in order to draft appropriate requirements and select the most promising sensing technology. The motivation of the rotor state measurement system within the MANOEUVRES project was the need to accurately estimate the main rotor blade flapping, and particularly its 1/rev (one per rotor revolution) cyclic components, as these are related to Tip-Path-Plane Angle of Attack (TPP-AOA) and therefore to the noise footprint [20]. Nevertheless, the system was designed to acquire the full blade motion, consisting in the coupling of the lag, flap and pitch angles, with the ability to catch higher-than-1/rev cyclic components.

The basic requirements for sensor system performance are reported in Table 1. They refer to the metrological performance necessary for accurate noise prediction, as well as for other possible uses, such as RSF control law applications.

Table 1: Measurement system performance requirements

Bandwidth	mandatory: 0-10 Hz	desired: 0-25 Hz
Accuracy	mandatory: 0.5 deg	desired: 0.1 deg
Range	lag: -13.5-10.3 deg	
	flap: -6.0-18.0 deg	
	pitch: -22.0-20.0 deg	

Furthermore, several additional requirements were considered, to specify the needs concerning functionality, geometry and mass characteristics, environmental suitability, reliability, safety, testability, and maintainability, aiming to a system appropriate for future airworthiness certification.

A wide variety of contactless technologies that could potentially satisfy these requirements was considered initially, with transducers pointing the rotor blades, based either on the fuselage or on the rotor hub. The types of sensing technologies initially evaluated are listed in Table 2.

In the technology review, capacitive, ultrasonic, eddy current, Hall effect, and magneto-inductive sensors were considered unfit, as they are potentially sensitive to environmental conditions, such as presence of dirt, moisture, water, and air turbulence. Also, eddy current, Hall effect and magneto-inductive types are typically characterized by limited measuring ranges and strong non-linearity, which impact on the measurement of arbitrarily coupled, large amplitude 3-D motions. Time-of-flight laser systems were also discarded because of their relatively low sampling frequency. As a result, 1-D and 2-D laser triangulation and vision systems were chosen as the most promising for candidate rotor state measurement system concepts.

Table 2: Preliminary technology selection

Type	**Installation**	
Capacitive	On rotor	
Ultrasonic	On rotor	
Eddy current	On rotor	
Hall effect	On rotor	
Magneto-inductive	On rotor	
1-D and 2-D laser triangulation	On rotor	On fuselage
Laser time of flight	On rotor	On fuselage
Vision systems	On rotor	On fuselage

This preliminary selection allowed conceiving possible architectures of the measurement system, where each technology was applied to different sensor and target locations. In particular, nine different concepts were drafted, with sensor placed either on the fuselage or on the hub, and targeting either the blade root, mid-span section or tip. Not only sensor size, weight and measurement range differ among the various concepts, but also many implications related to cost, helicopter requirements, technical challenge, technical capability and prospected commercial

exploitation. Therefore, an analysis was carried out, yielding three candidate systems, all based on the rotor hub and targeting the blade root: a 2-D laser scanner, a single camera system, and a stereo camera system. These measurement systems were all intended to be installed in the main rotor head, pointing to the target from above.

The following phase in the rotor state measurement system development involved a competitive evaluation of the concepts emerged from the previous analysis. Indeed, the three candidate systems were designed and implemented in full scale and, for each measuring solution, specialized algorithms have been developed for system calibration and real-time angle recovery. The evaluation of the most promising solution was based on a thorough experimental campaign carried out on test rigs at both the Politecnico di Milano laboratories and Leonardo Helicopters. Three types of tests aimed at the verification of the transducer functionality and actual capability were performed, assessing the ability of all systems to sustain vibration and centrifugal loads, and to satisfy the measurement accuracy requirements. The key parameter for the selection of the final solution was the measuring accuracy, which appeared to be higher for the stereoscopic vision system. Early work showed that for stereo camera system, the discrepancies of the three angles were comprised between 0.1^0 and 0.3^0 involving test rigs at Leonardo Helicopters Laboratories. This was eventually chosen as the most appropriate measuring solution for the application considered in the MANOEUVRES project. This activity is described in detail in [31].

3 Measurement approach

The main rotor of the target helicopter (AW139) has five blades and is fully articulated, with elastomeric bearings to permit lag, flap and pitch movements. To estimate the motion of the blade it is therefore necessary to measure the three mentioned angles. Lag, flap and pitch angles are defined with respect to the coordinate system X_f, Y_f and Z_f, integral with the hub (Figure 1). The center of the fixed reference system X_f, Y_f and Z_f coincides with the center of the elastomeric hinge that connects the blade to the hub. The X_f direction points to the tip of the blade. The Z_f direction is vertical to the surface of the hub towards the ground. The $-Y_f$ direction is determined by the cross product of X_f and Z_f.

The working principle of the blade angles measuring system is based on tracking the features of an appropriate target integral to the blade root [31]. The kinematic model of the blade motion with respect to the hub is represented by

$$P_f = R_c(\xi,\beta,\theta)\, P_{f0} \qquad (1)$$

where R_c represents the rotation matrix of the blade resulting from the three partial rotations for lag angle ξ, flap angle β, and pitch angle θ, respectively. The current 3-D position of each target feature expressed in the fixed reference frame is defined as P_f. When the three blade angles are equal to zero, the same coordinates are defined as P_{f0}. Therefore, the problem lies in the inversion of Eq. (1), which amounts to finding R_c from the knowledge of P_f and P_{f0}. When the rotation matrix is retrieved, the three blade attitude angles are found easily from rotation theory.

A stereo camera system is applied for the measurement of the target features. The layout of the system is displayed in Figure 1. A target with eight black disks on a white background is attached on the surface of the tension link, which is rigidly connected to the blade root and is connected to the hub by means of an elastomeric bearing. The cameras of the stereo system point to the target. The triangulation method [32] is then applied for a pair of images acquired by the left camera and the right camera to reconstruct the positions of the centers of the eight disks in the left camera coordinate system (X_L-Y_L-Z_L), while the parameters of the camera are calibrated by means of the Zhang method [33]. The positions of the captured features in the left camera coordinate system are converted into the positions P_f in the fixed coordinate system (X_f-Y_f-Z_f) by means of the transformation relationship, which is obtained through a calibration procedure. Considering the initial position, P_{f0} is known from the configuration of the setup and the target pattern.

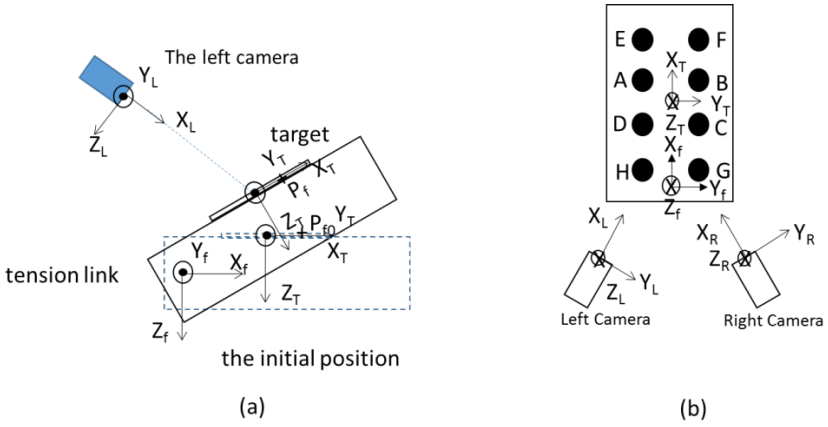

Fig 1. Sketch of the stereo camera measurement system with the adopted optical target

3.1 Motion recovery

In order to estimate the three angles of the blade, it is necessary to invert Eq. (1), finding $R_c(\xi,\beta,\theta)$. However, during flight, the centrifugal and lift forces inevitably generate a deformation of the elastomeric link that connects the blade root to the hub. This means that, in addition to the blade rotation to be estimated, there is a translation between the original position P_{f0} and the current position P_f. Moreover, the position of the centroids of the disks composing the

target is corrupted by noise, due to the large vibration level characterizing the main rotor of a helicopter. Although the camera support was developed and tested to reduce the camera-to-target vibrations to the minimum, it is not possible to eliminate this disturbance completely. Because of both blade translation and noise on image data, the inversion of Eq. (1) is not trivial. In [31] this inversion has been implemented relying on the estimation of the pseudoinverse of the rotation matrix. The results in [31] were satisfactory, however an approach based on the Singular Value Decomposition (SVD) is expected to provide a further increase of the estimation accuracy and robustness, also in the presence of blade translation and noisy measurements [34]. In this work, the approach based on the SVD technique is implemented and its performance is compared with the results of the approach based on the pseudoinverse matrix. The procedure to estimate the blade angles with the SVD procedure is summarized hereafter:

1. Compute the center of gravity of both the initial disks cloud P_{f0} and the disks in current position P_f:

$$\overline{P_{f0}} = \frac{\sum_{i=1}^{n} P_{f0i}}{n}, \overline{P_f} = \frac{\sum_{i=1}^{n} P_{fi}}{n}$$

2. Subtract the coordinates of the center of gravity from the coordinates of each disk:

$$X_i = P_{f0i} - \overline{P_{f0}}, Y_i = P_{fi} - \overline{P_f}$$

3. Compute the covariance matrix H as follows:

$$H = \sum_{i=1}^{8} X_i Y_i^T$$

4. Compute the Singular Value Decomposition of the matrix H:

$$H = U \Lambda V^T$$

5. Estimate the rotation matrix R as follows:

$$R = V \begin{pmatrix} 1 & 0 & 0 \\ 0 & 1 & 0 \\ 0 & 0 & \det(VU^T) \end{pmatrix} U^T$$

To compare the performance of pseudoinverse and SVD methods, the two techniques have been applied to process the results of experimental tests developed on a test rig available at the Leonardo Helicopters laboratories. This rig is composed of a subassembly of the AW139 helicopter main rotor components and is capable to impose arbitrary motions to the blade within the full operational range of blade angles. This includes the simulation of realistic time histories, with a full coupling of lag/flap/pitch blade angles. The test rig retrieves a reference measurement of the imposed angles, so that the output of the vision-based system under test can be compared with the reference data. The experimental tests developed on this rig have been described in [31]. In this work, such tests allowed evaluating the measurement accuracy in the actual geometrical configuration envisaged for the target helicopter application, using the approach based on pseudoinverse matrix. In this paper, the method based on the SVD is used to retrieve the blade

angles and the accuracy of the results is compared with the ones obtained with the pseudoinverse technique. For this comparison, the cases of realistic blade motion corresponding to four different trimmed level flight conditions at increasing airspeed values V_1, V_2, V_3 and V_4 are used (the actual airspeed values are not disclosed due to confidentiality obligations).

The estimated mean values of the blade angles do not significantly differ for the two computation methods: for both of them and for all the realistic flight conditions, the discrepancies of lag, flap and pitch angles are below 0.3°.

However, as the first harmonic component of the blade angles is a fundamental parameter to estimate the TPP-AOA, the comparison has been made also for this component. Figure 2 shows the discrepancy of the first harmonic of lag, flap and pitch angles in case of increasing airspeed conditions.

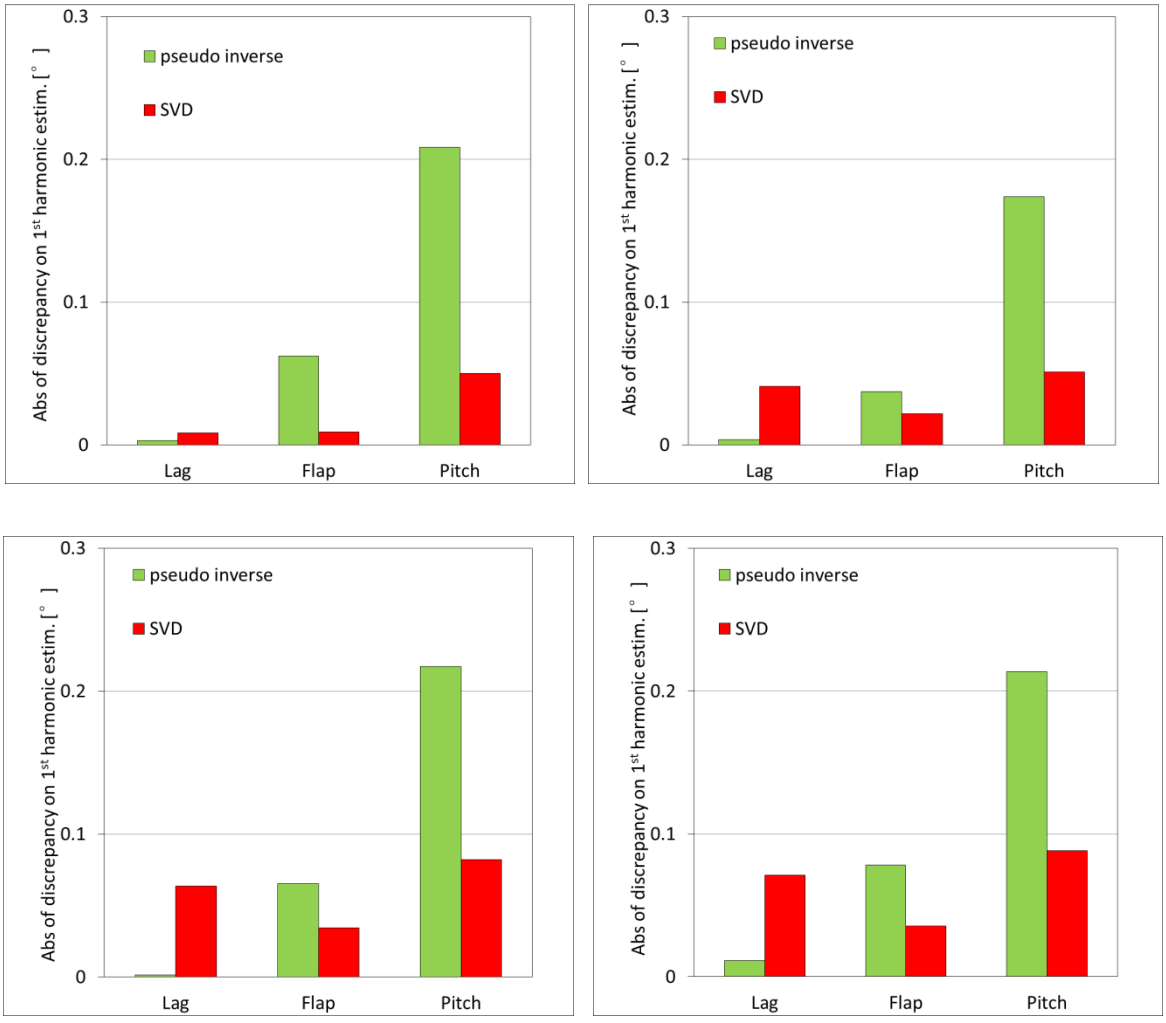

Fig 2. Discrepancy of the first harmonic of lag, flap and pitch angles in case of increasing airspeed conditions: V_1 top left, V_2 top right, V_3 bottom left and V_4 bottom right, with $V_1<V_2<V_3<V_4$

As shown, the discrepancy on the first harmonic for the lag angle is larger in the case of SVD. However, it is acceptable, since it is well below 0.1°. For the flap and pitch angles, the SVD method shows a relevant reduction of the discrepancy, therefore the solution based on this approach has been selected in the end.

3.2 Disk matching algorithm

The estimation of the 3-D coordinates of each of the eight disks shown in Figure 1b is obtained through a stereoscopic triangulation based on acquired images of the target. However, to run the triangulation, it is necessary to correctly couple each disk in the left image with the corresponding one in the right image without ambiguity. In the scientific literature, a wide number of stereoscopic feature matching algorithms are available [35]. However, these algorithms are based on image rectification and features detection, therefore they require a computation power that is typically unavailable in compact image processing units compatible with the installation on a helicopter rotor [36]. On the other hand, it is possible to develop disk matching algorithms customized for specific target types. These algorithms rely on the knowledge of the target characteristics and are either based on separating the disks into a left and a right group by increasing the horizontal spacing of the disks [31], or on creating a straight line by means of least-square fitting of centroid coordinates. These implementations are characterized by a low computation effort, however, do not work well in this application for some angular positions of the blade, in particular when large blade angles generate a severe perspective effect. For example, the method used in [31] fails when the horizontal coordinate of disk F is smaller than the horizontal coordinate of disk H - which can happen in the case of large pitch and flap angles, as in the example shown in the top graphs of Figure 3. On the other hand, the method based on the least square fitting of the centroids can fail when severe perspective conditions do not allow estimating the target orientation in the image using a linear fitting, as shown in the bottom graphs of Figure 3.

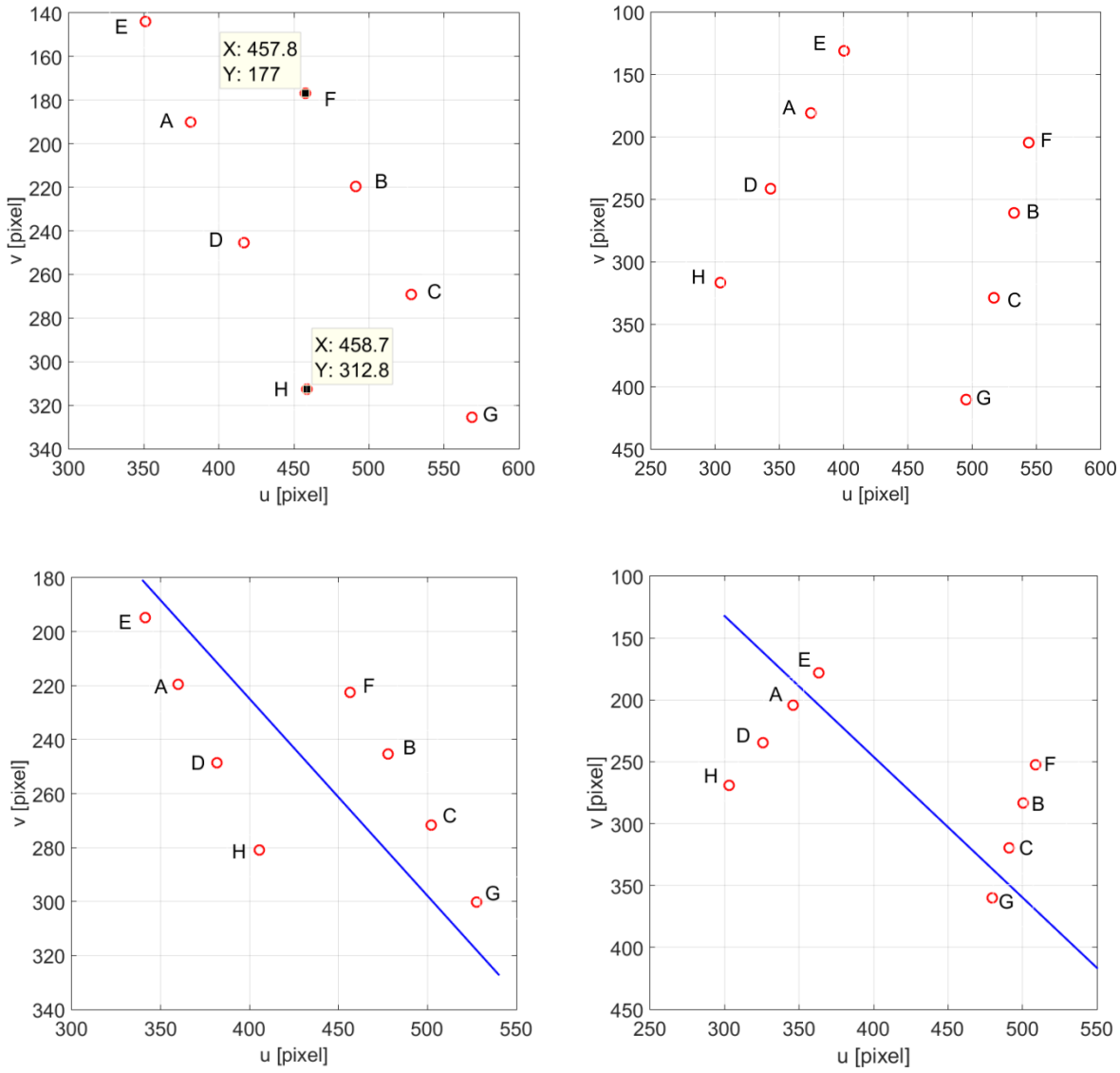

Fig 3. Examples of wrong classification: top graphs refers to blade angles for test #18 of Table 3, with matching algorithm used in [31], bottom graphs refers to blade angles for test #6 of Table3, with matching algorithm based on blob fitting

In order to correctly match each disk in all applicable blade positions, a customized disk matching algorithm is proposed. This algorithm is optimized for the specific pattern shape adopted in this work and it allows recovering the correct disk matching in any physically realizable position of the target for the present application. The basic idea is to create a straight line (termed 'splitting line') in the middle between the left group of the disks (E, A, D, H) and the right group of the disks (F, B, C, G) using a robust approach (see Figure 4). Then, the order of each group of disks is determined through the vertical coordinates of the disks. Finally, the disk pairs are matched.

For the creation of the splitting line, two points are needed. In this approach, the first point is represented by the center of gravity of the eight disks (point I in Figure 4). The second point (point J in Figure 4) must provide the direction of the splitting line. This is determined as the mid-point of two disks, named D1 and D2 belonging to the left group and the right group, respectively. The following steps are applied:

1. Disk D1 can easily be found as the leftmost disk in each image. Therefore, point E is detected in the left image and point H in the right image and named D1.
2. To select disk D2, choosing the rightmost one is not convenient, as in this case point J (the mid-point between D1 and D2) would fall very close to the center of gravity I. Therefore, the estimated direction of the splitting line would not be robust. Hence, disk B or C should be selected as D2. As a matter of fact, for large blade angles, in the left image disk F could fall at the left of I, and disk H could fall at the right of I. The same problem might happen with disks E and G in the right image. Therefore, to be sure that disk B or disk C is selected, it is necessary to choose the third disk to the right of I as D2.
3. Point J is computed as the mid-point of D1 and D2.

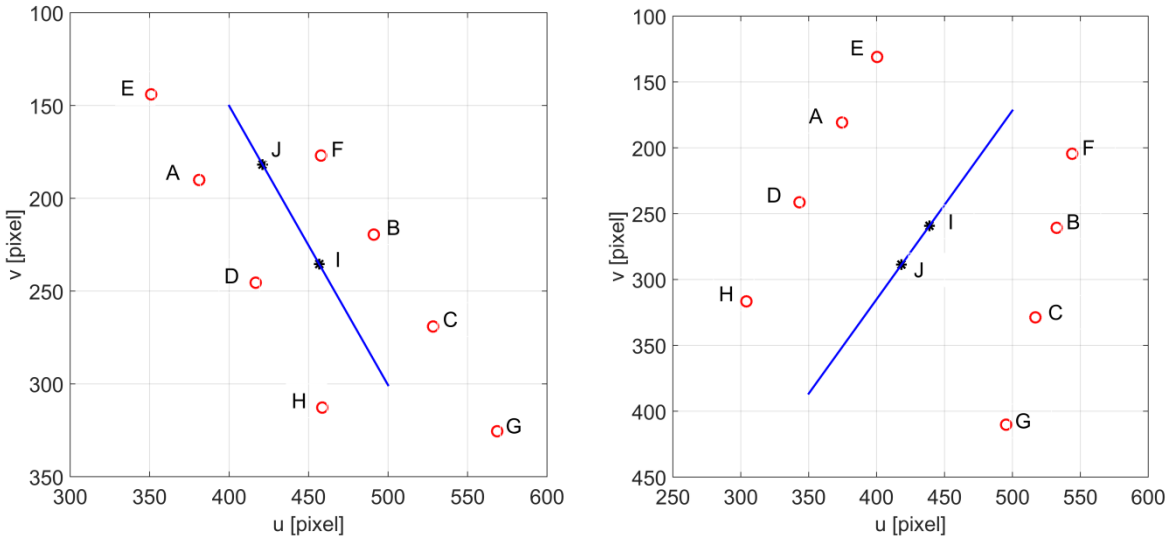

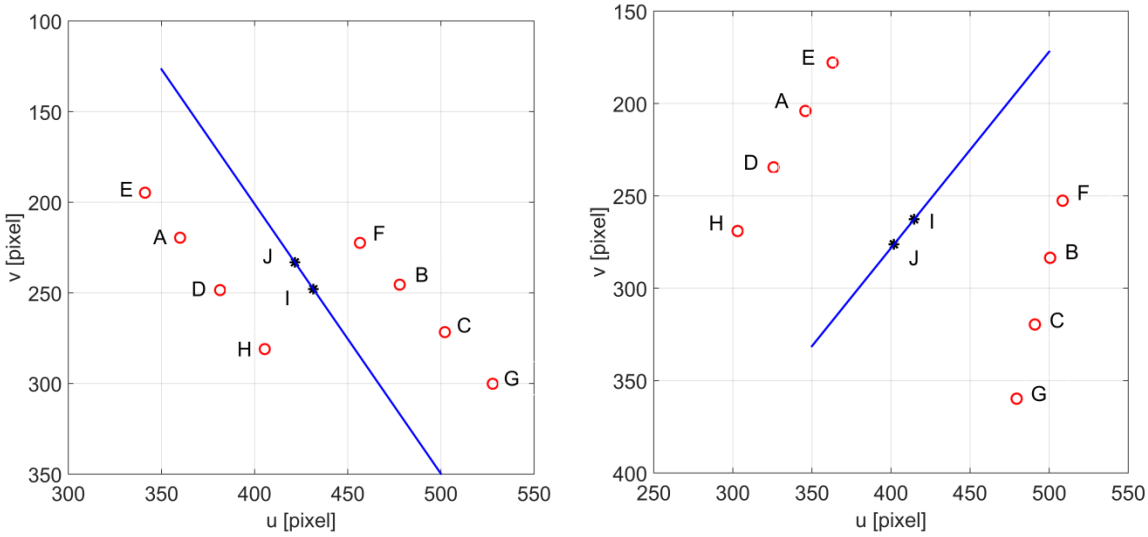

Fig 4. Correct blob classification obtained applying the matching algorithm proposed in this work to the same conditions shown in Figure 3

Figure 4 shows an example of the matching result in the same cases shown in Figure 3. The proposed disk matching algorithm correctly sorted the disks in the two stereoscopic images, showing good robustness and allowing to find the correct disk match for all the realistic blade conditions considered in the next section.

4 Measurement system description

The measurement system is composed of a stereo camera, a lighting device, a Trigger Generator (TG), and a Trigger Distributor Unit (TDU), as shown in Figure 5. These components are integrated on a helicopter main rotor 'beanie', a hat-shaped device placed on top of the rotor hub, together with the necessary wirings and a processing unit for motion recovery. As seen in Figure 5, the TDU not only converts the trigger signal from the TG and conveys the power for the camera and the lighting device from the external power supply, but it also transmits acquired data from the cameras to the acquisition computer. Since camera data are sent to the computer via an RS422 protocol, the latency in the transmission is not negligible. Therefore, the trigger signal is also recorded by the computer, to insure the knowledge of the exact image acquisition time.

4.1 Stereo camera system

The cameras selected for the rotor state measurement system prototypal device are two Teledyne Dalsa BOA200 Pro with a sensor resolution of 640 x 480 pixels. This camera model was one of the smallest smart cameras available on the market at the time the system was developed. Smart cameras were considered as they are equipped with an internal

CPU that allows them to run image-processing algorithms. This is fundamental for the present application, because it substantially decreases the amount of data to be transmitted from the rotating system (the main rotor hub) to the acquisition computer, hosted in the fuselage. Thanks to the on-board processing capabilities, the smart cameras allow analyzing the acquired images in real time and sending only the coordinates of the centroids of the eight disks of the target (i.e. 16 numbers) to the computer, instead of transmitting all the image data (approximately $3 \cdot 10^5$ gray values). This also permits the increase of the system acquisition frequency, allowing it to obtain higher-than-1/rev components of the motion of the blades. Moreover, the small size of the cameras is a key point in easing the system integration within the beanie, where the space available is very limited.

In order to acquire an appropriate field of view, the camera model with 4.5 mm focal length optics with C-mount connection is used, therefore reducing the risk of missing the target in the case of large motion conditions. The exposure time of the cameras is set at 10 µs, in order to reduce the influence of the motion blur. An array of four Philips Lumileds LXK8-PW40-0016A devices is applied to provide adequate illumination of the target. To reduce power consumption and self-heating, the LEDS are operated in strobe mode. The stereo camera system and the lighting device are synchronized by means of the trigger distributor unit (Figure 5).

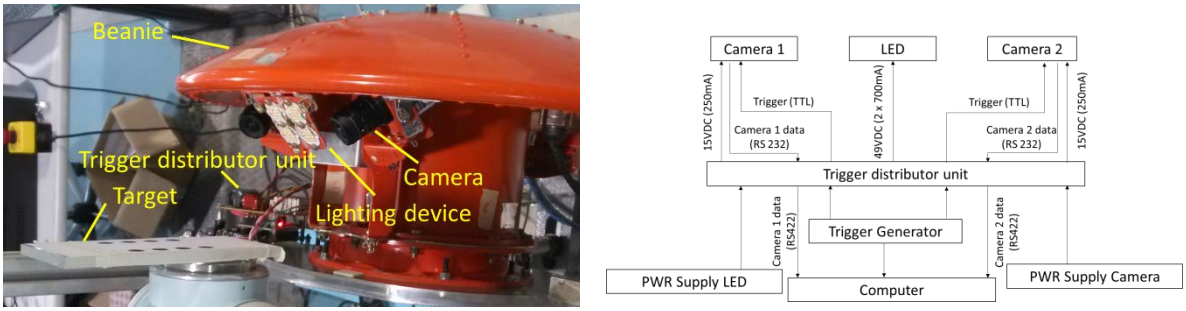

Fig 5. Arrangement of the measurement system

4.2 Trigger Generator and Trigger Distributor Unit

The TG and the TDU are custom-developed electronic units designed to interface the camera system with the rotorcraft and the data acquisition computer. The TG, as the name suggests, is used to generate the *N*/rev trigger signal and to transmit it to the TDU through a slipring mounted on the main rotor shaft.

The test helicopter features a constant speed main rotor, but since the loop is closed by the Full Authority Digital Engine Control (FADEC), fluctuations around the set-point rpm may occur in response of torque variations, which is

typically the case of maneuvering flight. Therefore, it was decided not to rely on the nominal main rotor rpm, but rather to measure it continuously, using the 1/rev 'beep' signal generated by an on-board sensor whenever a reference blade passes over the tail. The actual, measured period of a revolution is divided by N and used to generate the trigger for the following revolution, thus delivering a signal that triggers the camera system always at the same azimuthal position throughout a very wide range of main rotor rpm (50% to 150%). The N/rev trigger is then split and fed to the data acquisition system and to the TDU via a balanced line, in order to guarantee the sufficient signal integrity and reliability when passing through the slipring.

In addition to receiving the N/rev trigger from the TG and delivering it to the cameras and lighting device, the TDU performs some housekeeping tasks. Namely, it provides a stabilized power supply to all beanie-mounted systems (including the 49 V high voltage for the lighting device) and converts the single-ended RS 232 signal coming out of the cameras to the balanced RS 422 standard line.

The parameter N can be set to any arbitrary integer values in the TG: in this implementation it was set to 7, as discussed in the next section.

4.3 Implementation issues

The image acquired by the each camera at every trigger pulse is processed immediately on-board the camera, in order to detect and transfer the centroids of the disks (visible in Figure 1) to the computer in real time. On the computer, the blade angles are estimated by means of the measurement approach described in Section 3. Hence, the processing steps to be accomplished on-board the smart cameras are: image binarization, blob analysis to detect the centroids of the disks, and managing of the serial communication to the host computer.

To meet the mandatory bandwidth requirements stated in Section 2 (i.e. 0-10 Hz), the minimum acquisition frequency is 20 Hz. Therefore, since the nominal speed of the main rotor is close to 5 Hz for the target helicopter, the minimum number of images to be acquired per revolution corresponds to $M \cong 4$. A larger M value would allow to better analyze the dynamics of the blades and it is therefore desirable. However, the main limit to the increase of M is the computational time required by the smart cameras to perform the image processing of each acquired image and to manage the data transfer to the computer. In order to reduce the processing time and obtain the maximum possible value of M , the image processing steps were simplified as much as possible.

In particular, the image binarization was implemented with a fixed threshold value. Adaptive thresholding and locally adaptive thresholding algorithms ([37-38]) allow optimization of the results even in time and space varying illumination intensity, but the computation time is not compatible with the requirements of this installation and the available hardware resources. As for the blob analysis procedure, to reduce the computation time the correct blobs were selected among all the detected ones relying only on their area, without implementing more complex morphologic operations ([39-40]). To ensure a correct binarization and blob selection even with the mentioned limitations for software complexity, great care was posed in the optimization of the illumination uniformity. Also, the lighting devices were strobed synchronously with the cameras to obtain a higher lighting intensity. In this way, the effects of the huge variability of natural lighting conditions due to the rotation of the beanie were strongly mitigated, making the image processing more robust.

The last step performed by the smart cameras is the transmission of the centroid coordinates to the host computer. To reduce the bandwidth through the slipring and the transfer time, the coordinates of the centroids are converted into the minimum representation capable to convey this type of data, i.e. 2-byte format numbers. Data are then transferred to the computer by means of an RS-422 connection.

On average, the time required by the BOA200 PRO smart cameras to acquire an image and perform the computation steps described above is 20 ms. Because of the variability of this processing time and of the need of an additional time to arm the trigger, the maximum frame rate that can be ensured by the developed system with a negligible risk of missing frames is 35 Hz. Hence, the number of images per revolution that can be acquired is $N = 7$, as anticipated above.

5 Experimental validation campaign

In order to employ the measuring system described above in a flight test activity, it is fundamental to fully qualify its reliability and accuracy. To this end, the measurement system assembly was subjected to extensive laboratory testing to insure its suitability for on-board installation and to verify the satisfactory properties demonstrated in the preliminary test phase [31]. Naturally, special care was taken in assessing the safety of the integration on the AW139 beanie, to clear out possible mechanical failures or inconveniences of any kind. Furthermore, the measuring accuracy

was verified again, in order to insure the correctness of the software and hardware improvements carried out after the selection of the stereoscopic system for final development.

These goals were pursued through multiple test activities, separated in two categories. First, the assessment of the system suitability and functionality in the harsh environment involved by on-board operations was sought. These tests included modal characterization, vibration resistance, rotation resistance, and sunlight sensitivity. Second, accuracy tests were carried out exploring the complete range of possible blade positions. This involved measurements at a large number of target orientations, which is already a complex activity on a stationary testbench. Therefore, as harsh environment tests were carried out on vibrating and rotating rigs, no attempt was made to assess the accuracy during these tests.

In the following, the harsh dynamic tests and the accuracy tests carried out are described, while the next section focuses on the test outcomes.

5.1 Harsh environment tests

The goal of harsh environment testing was to take into account the main circumstances contributing to the operating conditions of any device installed aboard the main rotor hub of a flying helicopter. The test planning made the most from experimental resources present at the Politecnico di Milano, involving modal tests, vibration tests, and coupled vibration, rotation, and sunlight sensitivity tests. Figure 6 shows the experimental rigs and the setup for these tests.

5.1.1 Modal tests

The modal tests aimed at measuring the natural frequencies of the integrated system (Figure 6a) installed on the AW139 rotor head, in order to verify that no resonances may occur during flight operations. The modal analysis was conducted using a dynamometric hammer as an excitation technique. The response of the measuring system and of selected critical parts of the beanie was measured with nine accelerometers: five of them mounted on the cap of the beanie and the other four at the base of the cylinder. Further investigations were performed on various parts of the beanie by means of a low-mass accelerometer, in order to exclude the existence of other local modes of the added objects, such as cameras, balancing masses, and lights.

5.1.2 Vibration tests

The vibration tests aimed at imposing on the whole measuring system a realistic vibration level for a predefined amount of time, in order to check whether any of the parts of the system may undergo failure or mechanical loosening that might be dangerous during flight. For the vibration tests (see Figure 6b), the integrated system was connected to an Unholtzdickie SA15-S452 electromagnetic shaker located in the laboratories of the Department of Mechanical Engineering at Politecnico di Milano. The integrated system was instrumented with three tri-axial accelerometers. Two of them were placed on the two cameras, in order to record the response to vibrations, while one was fixed on the top of the beanie, in order to verify the correspondence of the supplied vibration to the desired one. The vibration applied to the system was characterized by a spectrum equivalent to the one recorded on a AW139 during forward flight at 165 kn and during a landing flare maneuver, using a tri-axial accelerometer placed on the helicopter main rotor hub.

5.1.3 Coupled rotation and vibration tests

These tests aimed at verifying that the integrated system was capable of resisting to realistic centrifugal loads coupled with gearbox-generated vibrations without showing the occurrence of structural problems. For these tests, the beanie was mounted on the spinning hub of an A109MKII ‘ironbird’ available at the laboratories of the Department of Aerospace Science and Technology, Politecnico di Milano. This complex test rig, partially visible in Figure 6c, was developed using the fuselage, the gearbox, and the main rotor mast of an Agusta A109MKII helicopter [41]. Therefore, it was possible to reproduce a highly realistic dynamic behavior of the main rotor subsystem. The target was fixed in front of the measuring system in a representative position and multiple data acquisitions (lasting 5 min each) were conducted to check the stability of the measurements.

5.1.4 Sunlight sensitivity tests

Sunlight sensitivity tests were carried out to check the robustness of the developed measuring system against the dazzle of the cameras due to sunlight. Again, the A109MKII ironbird was employed, in order to achieve maximum representativeness. The sunlight was simulated with a calibrated light source simulating the natural sunlight intensity placed near the rotor during rotation. Sunlight effect on the measurement results depends on the position of the light source simulating the radiation of the Sun and, for a minor part, on target attitude. The key parameter is the relative angle between the sunbeam and the optical axis of the camera. We considered a priority to conduct the sunlight tests

with an actually rotating system, in order to check the sunlight effect when the measuring system undergoes to the same dynamic fluctuation of light intensity that will have to endure in a real flight condition. Therefore, we mounted the measurement system on the A109MKII ironbird for the sunlight sensitivity tests. With this arrangement, which does not include a main rotor head with its articulations, it was simply too complex to provide the ability to change the attitude of the target with respect to the measuring system. A significant issue, impacting on safety, is connected with adequate inertia balancing. Therefore, we limited this investigation to the exploration of the effect of the relative angle between sunbeam and stereo cameras by modifying the position of the sunlight simulator. The light was placed in three different positions, simulating three representative orientations of the Sun relative to the measurement system:

1. Upper position, with an inclination of about 45° above the hub plane: this allowed illuminating the target at an angle (see Fig 6d.);
2. At the height of the cameras (light source lying in the hub plane): which provided unequal illumination of both target and camera lenses;
3. Lower position: this was chosen in order to directly point the light beam towards the camera lenses.

Fig 6. Harsh dynamic tests: (a) modal tests; (b) vibration tests; (c) rotation tests and sunlight sensitivity tests; (d) sunlight sensitivity tests, with the calibrated light in the upper position

5.2 Accuracy tests

The aim of these tests was to impose a set of different positions and orientations on the 8-disks target, simulating realistic rotations of the target up to the maximum angular range of pitch, lag and flap of interest. For this purpose, a seven-degrees-of-freedom robot arm was employed to simulate the motion of the target on a real blade, respecting the kinematic constraints enforced by the elastomeric bearing that connects the blade to the main rotor hub. Figure 7 shows the test rig developed. The relative position between the beanie and the target was nominally equal to the one that characterizes the real layout of a helicopter, so as to ensure that the stereoscopic system can grab images of the target in the realistic 3-D position and orientation.

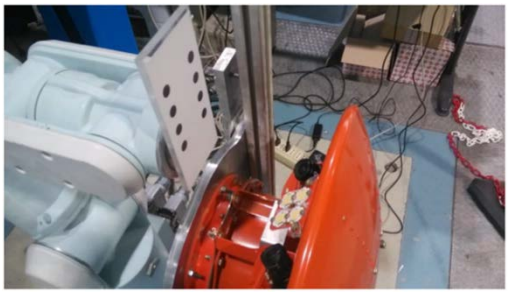

Fig 7. The measurement system based on a stereo camera integrated with a helicopter beanie

5.2.1 Design of the angular positions tested

The goal of accuracy tests was to qualify the developed measuring system in the whole blade working range of motion. The maximum values for each blade angle were extracted from measured flight conditions up to an airspeed of 160 kn. To explore a worst-case scenario in terms of combined ranges, the maximum and minimum values of the three angles were grouped in all possible combinations, regardless of the fact that some of the positions tested may not be actually achievable in flight, as typically not all maximum or minimum values for the three angles are reached at the same time. Table 3 shows the list of the angular positions imposed on the target during the accuracy tests.

Table 3 List of all angular positions tested in the accuracy tests

Test#	Lag (^{0})	Flap(^{0})	Pitch(^{0})
1	3	0	0
2	-3	0	0
3	0	-2	0
4	0	8	0
5	0	0	-8

Test#	Lag (^{0})	Flap(^{0})	Pitch(^{0})
21	-3	8	-8
22	-3	8	21
23	3	-2	-8
24	3	-2	21
25	3	8	-8

6	0	0	21	26	3	8	21
7	3	-2	0	27	0	-4	-8
8	3	8	0	28	0	-4	21
9	-3	8	0	29	0	12	-8
10	-3	-2	0	30	0	12	21
11	3	0	-8	31	-6	-4	-8
12	3	0	21	32	-6	-4	21
13	-3	0	-8	33	-6	12	-8
14	-3	0	21	34	-6	12	21
15	0	-2	-8	35	6	-4	-8
16	0	-2	21	36	6	-4	21
17	0	8	-8	37	6	12	-8
18	0	8	21	38	6	12	21
19	-3	-2	-8	39	0	12	0
20	-3	-2	21	40	0	-4	0

5.2.2 Pattern optimization

The diameter and the relative distances between disks play an important role in the performance of the measuring system. The larger the target, the better the measuring accuracy. However, with a larger target some disks can fall off the boundary of the field of view. Therefore, the detection of the centroids is affected by a larger uncertainty, due to the imperfect illumination of the peripheral area. In the worst cases, a blob close to the boundaries of the field of view may be missed, or wrong blobs may be found instead. If the situation occurs, the corresponding measurement is not correct. The optimization of the size of the target is therefore the result of a tradeoff between the accuracy of the measurement and the need to robustly detect all of the blobs. Three sizes of the target were considered for accuracy tests (Figure 8). The pattern types considered are the following:

1. Pattern A: 25 mm spacing between disks and 12 mm disks diameter (L_1=25 mm and L_2=12 mm);
2. Pattern B: 20 mm spacing between disks and 12 mm disks diameter (L_1=20 mm and L_2=12 mm);
3. Pattern C: 15 mm spacing between disks and 10 mm disks diameter (L_1=15 mm and L_2=10 mm).

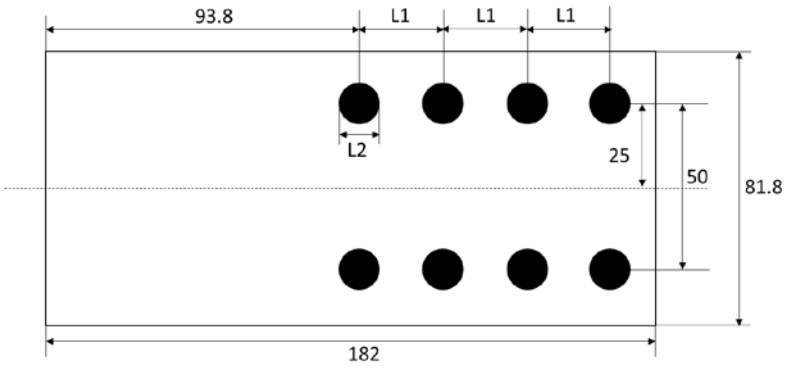

Fig 8. Pattern configuration

6 Discussion of results

6.1 Harsh dynamic tests

The modal tests allowed the Frequency Response Functions (FRFs) of the most critical parts of the assembly to be measured in the range of 0-512 Hz, with a frequency resolution of 0.25 Hz. Each point was hammered 10 times, in order to reduce measuring noise through averaging. The identification was carried out with the software LMS-Test.Lab Rev.13A, which uses the Polimax algorithm. Coherence analyses of the acquired signals showed values very close to 1 throughout the acquired bandwidth. Therefore, the excitation was considered suitable for test purposes.

The global response of the beanie obtained in the modal tests is dominated in the low frequency bandwidth by a mode around 152 Hz (see Figure 9a, where the sum of FRFs is shown). The spike in the response at about 50 Hz was carefully examined: it does not correspond to a global mode of the structure; it is a local mode of the upper part of the cap of the beanie (this was previously used in many flight test activities developed by Leonardo Helicopters), and does not affect the measuring system dynamic response. Relying on the experimental data acquired in previous flight tests by Leonardo Helicopters with an AW139 aircraft (target machine for the future flight test campaign), it is known that the vibration exciting the beanie is mainly in the frequency range below 100 Hz. Therefore, the frequency response of the instrumented beanie can be considered satisfactory for the installation on this helicopter.

The results of the vibration tests for the integrated system were assessed on the basis of the following criteria: verification of the tightening of the screws, verification of the position of the optical assembly (photographic lens, cameras, etc.), verification of the structural integrity (no cracks, no missing parts, etc.) and verification of the

functionality of the measurement. The check was positive for all the criteria. Moreover, the system acquired data on a continuous basis and the measurement showed no influence of the vibration conditions on data stability. The same criteria were used to evaluate the results of the rotation tests, and the check was again positive for all the criteria. Moreover, during the rotation tests, the output of the measured system was acquired by means of a customized wi-fi data communication system: the measurement was acquired continuously and did not show any significant influence of the rotation and vibration conditions on data stability.

The internal cabin equipment is usually tested using a light intensity of 108,000 lx, in order to verify that it can be correctly seen by the pilot even when illuminated directly by the Sun. Indeed, this value corresponds to the direct sunlight illumination attenuated by the cabin window glass by 20%. Therefore, the sunlight sensitivity tests were performed with a light source generating 135,000 lx on the measuring system, corresponding to a non-attenuated illumination.

The results of the sunlight sensitivity tests were very encouraging, showing a very low influence of the sunlight on the measurement functionality. In particular, when the light is placed in the upper position, pointing directly to the target, no data loss is observed. For the case when the light is in the middle position, one datum every 1,000 is lost. For the case when the light is in the lower position, directly pointing towards the camera, one datum per revolution is lost due to local saturation (Figure 9b). Therefore, in general, the system performance is basically unaffected by sunlight, while in the worst situation, it is slightly degraded. During sunlight sensitivity tests the target was mounted in a fixed position with respect to the hub, therefore the blade angles were nominally constant. The vibration of the target and of the cameras leads to a variability of the estimated angle values. Standard deviation of the estimated angles represents the type-A uncertainty of the measurement (defined according to [42]). However, while the vibration of the cameras represents a source of uncertainty for the developed stereoscopic system, the vibration of the target is only due to the response of the structure that connects the target to the hub of the ironbird. Hence, the standard deviation of the blade angles represents an overestimation of the measuring uncertainty, corresponding to 0.02°, 0.03° and 0.08° for lag, flap and pitch angles respectively.

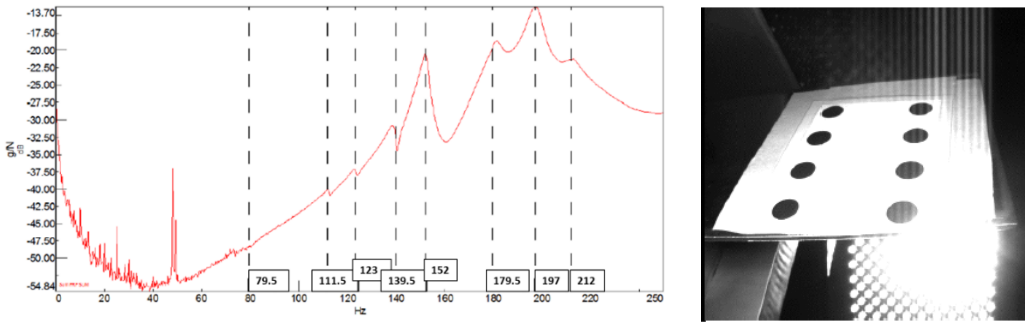

(a) (b)

Fig 9. Partial results of harsh dynamic tests: (a) Modal tests: Sum of FRF for all excitations; (b) Sunlight sensitivity tests: Right camera

6.2 Accuracy tests

Figure 10 shows the results of the acquisitions for all angular position cases included in Table 3 using the original target geometry (Pattern A). The instances of large errors in the results (angles that are estimated in a completely wrong way) are either due to one disk missing or to a disk wrongly detected. This aspect is analyzed in the following section, together with the description of the recovery actions applied. Note that if one disk is not detected and no other blobs are found in the image, the software conventionally assigns coordinates (0,0) to one blob to keep track of the error. Figure 11 shows an example of a wrongly detected disk: one disk is missing, while another spurious blob is detected. In tests with pattern A, 12 angular conditions out of 40 showed error due to wrong detection.

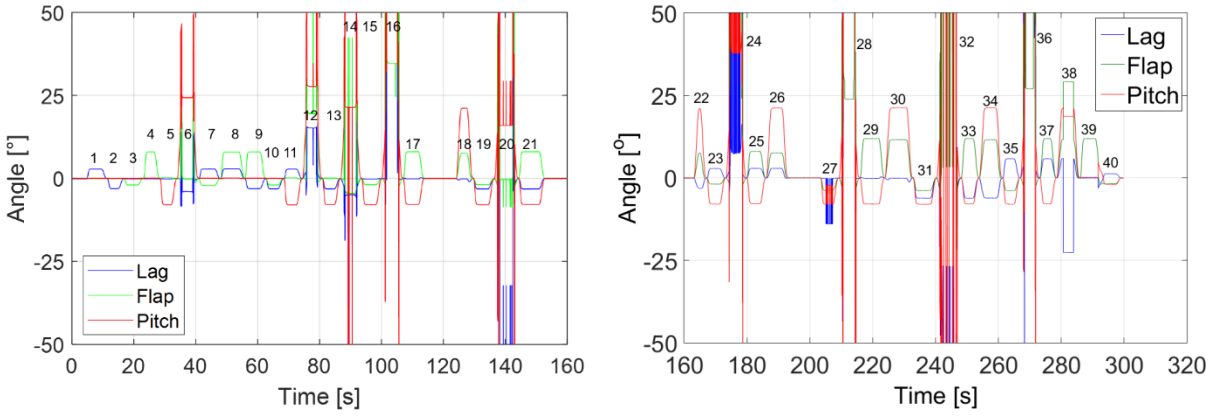

(a) (b)

Fig 10. Acquisition results of Pattern A target: (a) cases from 1 to 21; (b) cases from 22 to 40

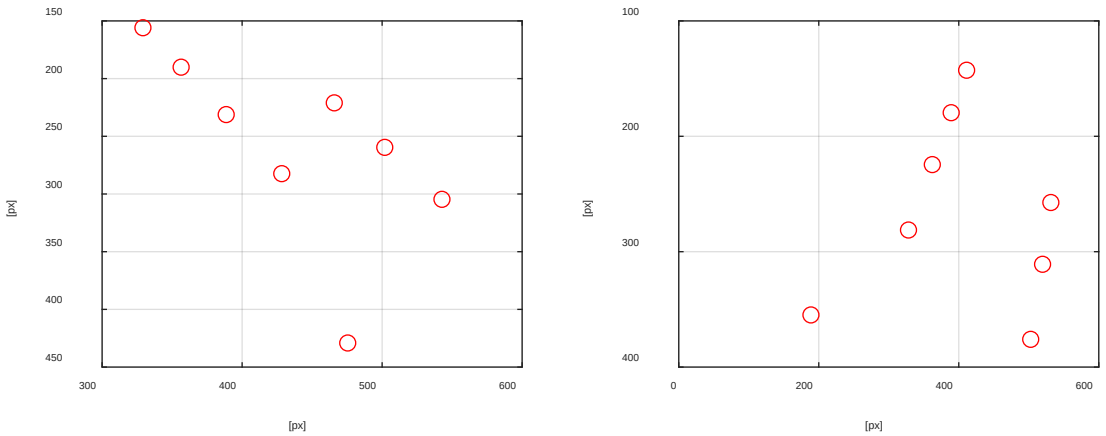

(a) (b)

Fig 11. Error in the detection of one blob: (a) case 6: left camera; (b) case 6: right camera

Figure 12 shows the results obtained with the first modified geometry (Pattern B). Again, the number of errors due to one missing disk or to a wrong detection is quite large: 8 conditions out of 40.

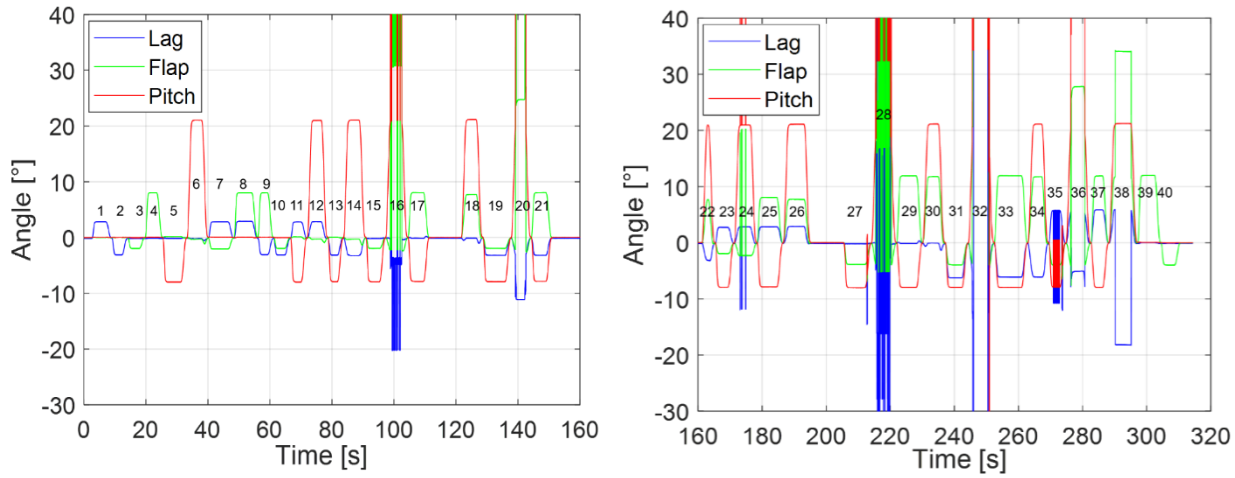

(a) (b)

Fig 12. Acquisition results of Pattern B target: (a) cases from 1 to 21; (b) cases from 22 to 40

Figure 13 shows the results obtained with Pattern C. In this case, the errors due to a missing disk or a wrongly detected disk are just three.

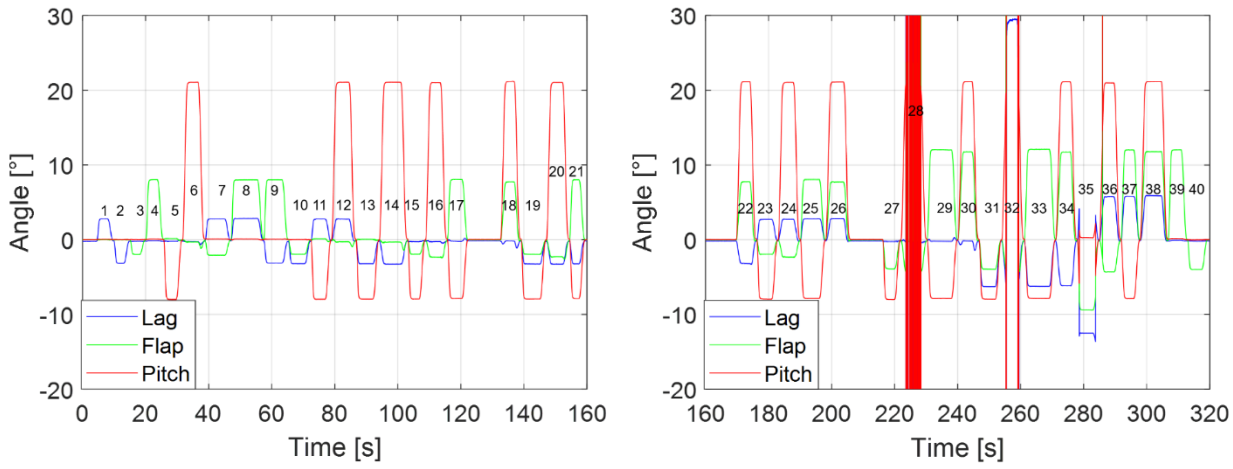

(a) (b)

Fig 13. Acquisition results of Pattern C target: (a) cases from 1 to 21; (b) cases from 22 to 40

For Pattern A, once a large pitch occurs, even in the case of pure pitching motion such as in case 6, a wrong blob detection is observed. Although for Pattern B the spacing value is reduced to 20 mm, the bad cases are not strongly reduced. In most of the cases, a wrong measurement occurs when coupling three angles including large pitch values. For Pattern C, where disk spacing is further reduced, mistaken acquisition cases decrease remarkably. Wrong measurements are still present only in three cases, when large pitch angles are contemporarily applied to non-negligible flap angles (#28, #32 and #35).

In the case of Pattern C, the incidence of wrongly detected blobs is limited, and no more than one blob is missing in each couple of stereoscopic images. In these conditions, it was possible to develop a more advanced version of the processing software, capable to recognize possible wrongly detected blobs, to ignore them, and proceed with the estimation of the blade angles with the seven correctly detected blobs. This improvement was found to be crucial in the subsequent on-board testing activities.

6.2.1 Discrepancy of the angular data obtained with different target types

Figure 14 shows the error in the lag, flap and pitch angles for the three different types of target, while the maximum minimum and mean error values can be found in Table 4, together with the number of target position where wrong blob detection happens. The main factor resulting in these error values is likely due to the non-perfect uniform lighting obtained with the LED illuminators used in this application. In particular, the disks that lie farther from the lighting

device, appear darker than those closer to it. Therefore, different disks appear with different brightness and contrast with respect to other disks. This phenomenon affects the estimated position of the disks, because some regions of the disks may be eroded.

By comparing the results shown in Figure 14, it is clear that the size of the target is reduced and the error on the blade angle estimation does not change significantly. However, for the flap and pitch angles, a smaller target area somewhat reduces the error. This is reasonable, due to the fact that, with a smaller target area, the disks are included in an area that is better illuminated. Therefore, the uncertainty in the detection of the position of the centroids is lower than in the case of larger target areas.

Table 4: Maximum, minimum and mean error on the lag, flap and pitch angles for the three pattern types

	Pattern A: 12 wrongly detected blobs		
	Lag Error [°]	Flap Error [°]	Pitch Error [°]
Max	0.00	0.22	0.25
Min	-0.22	-0.45	-0.03
Med	-0.16	-0.06	0.07
	Pattern B: 8 wrongly detected blobs		
	Lag Error [°]	Flap Error [°]	Pitch Error [°]
Max	0.02	0.15	0.16
Min	-0.24	-0.32	-0.04
Med	-0.16	-0.05	0.05
	Pattern C: 3 wrongly detected blobs		
	Lag Error [°]	Flap Error [°]	Pitch Error [°]
Max	0.00	0.13	0.19
Min	-0.28	-0.36	-0.01
Med	-0.21	-0.08	0.08

Since both the type and position of the lighting device represent fixed constraints at this stage of the work, it is concluded that Pattern C provides the best solution. Furthermore, Pattern C performs much better in terms of wrongly detected blobs. The absolute value of the discrepancy between imposed and measured angles, excluding the conditions of wrongly detected blobs, is always lower than 0.36° for all angles in the case of pattern C. These results appear promising and favorably compare to those presented in [43], where a device capable of measuring the blade attitude by means of an array of Anisotropic Magnetoresistive (AMR) sensors on the rotor hub is considered. In this case, the

system tested in rather simplified test conditions, not involving fully coupled blade motions, shows a similar accuracy in flap angle, while a discrepancy up to 1° is reached in lag and pitch angles.

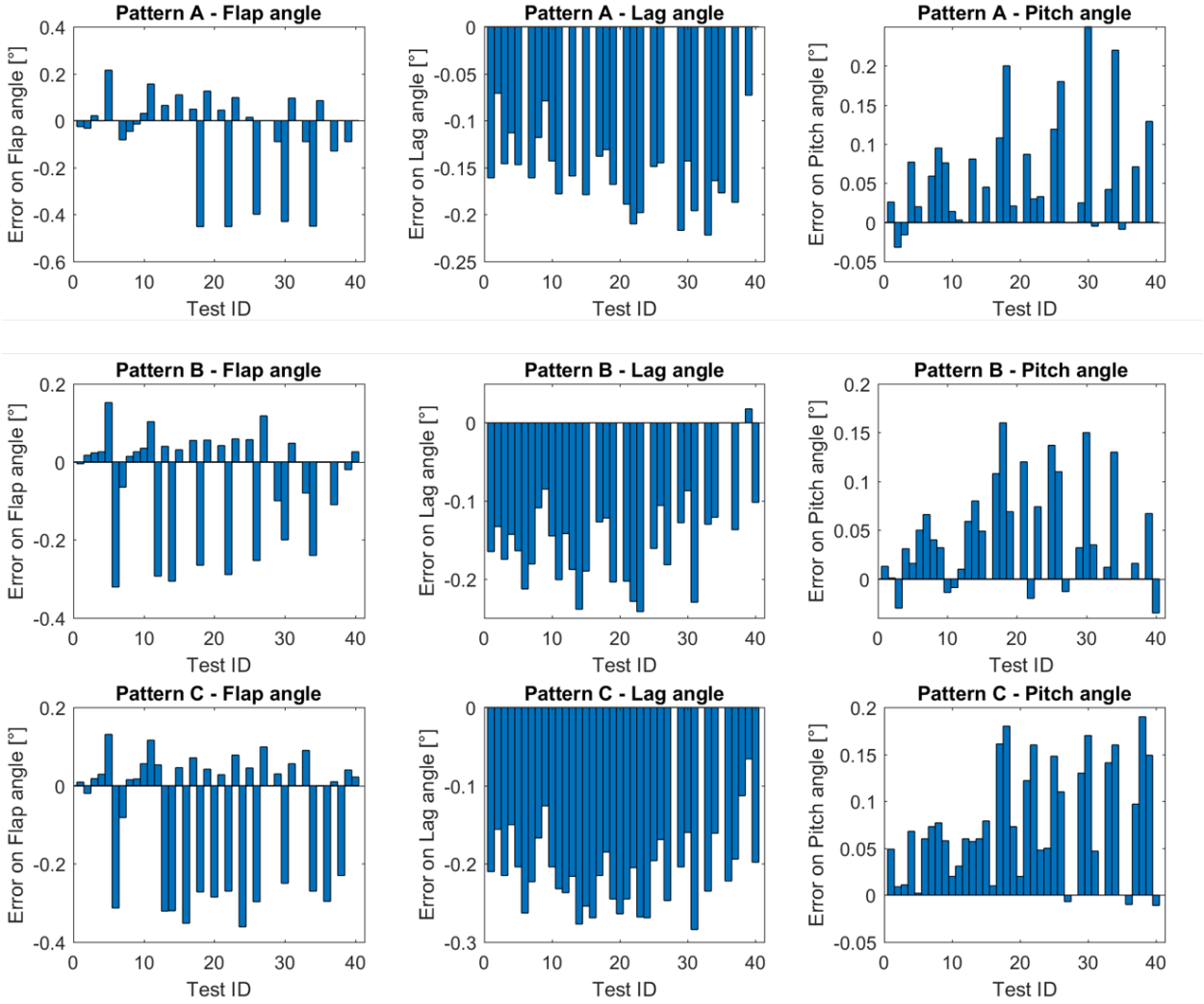

Fig 14. Error on the lag, flap and pitch angles for the three pattern types (missing bars denote missing data)

7 Conclusion

A novel rotor blade motion measurement system based on a stereo camera sensor integrated with a lighting device and a triggering equipment was developed and integrated within a helicopter main rotor head assembly, with the aim of measuring the attitude angles of a main rotor blade in real-time during flight. The measurement principle was validated by theory and extensive experiments, and implemented through several customized algorithms and dedicated hardware components, improving previous demonstrators in order to achieve a ready-to-fly prototype. A wide array

of laboratory experiments, including modal, vibration, rotation, and sunlight sensitivity tests demonstrated the ability of the integrated system to withstand realistic operational loads without any occurrence of structural damage or loosening of mechanical connections. Also, they insured that the system performs correct operations when subjected to the harsh working conditions found on board a helicopter rotor head during flight. Dedicated tests show that the accuracy of the developed measuring system is fully appropriate for blade angle measurement, even in the case of large, coupled angle combinations. These results are fundamental for the following activity involving ground and flight tests on board an instrumented AW139 prototype, in order to achieve the necessary clearance for installation and operation of the integrated system. A preliminary account of this final activity is given in [44] and will be discussed in detail in a future contribution.

Acknowledgement

The authors acknowledge the financial support provided by the MANOEUVRES project, framed within the Green RotorCraft (GRC) Integrated Technology Demonstrator of the European Union Clean Sky Joint Technology Initiative under Grant Agreement N. 620068.

References

[1] Prouty, R.: Helicopter performance, stability, and control. Krieger Publishing Company (2002)

[2] You, Y., Jung, S.N.: Optimum active twist input scenario for performance improvement and vibration reduction of a helicopter rotor. Aerosp. Sci. Technol. 63, 18–32 (2017)

[3] Gennaretti, M., Bernardini, G., Serafini, J., Romani, G.: Rotorcraft comprehensive code assessment for blade–vortex interaction conditions. Aerosp. Sci. Technol. 80, 232–246 (2018)

[4] Touron, M., Dieulot, J., Gomand, J., Barre, P.: A port-Hamiltonian framework for operator force assisting systems: Application to the design of helicopter flight controls. Aerosp. Sci. Technol. 72, 493–501 (2018)

[5] Wang, X., Cai, L.: Mathematical modeling and control of a tilt-rotor aircraft. Aerosp. Sci. Technol. 47, 473–492 (2015)

[6] Jimenez, G.A., Barakos, G.N.: Numerical simulations on the ERICA tiltrotor. Aerosp. Sci. Technol. 64, 171–191 (2017)

[7] Hanif, A., Yousaf, M.H., Fazil, A., Akhtar, S.: Inflight helicopter blade track measurement using computer vision. In: 2014 IEEE Region 10 Symposium 56-61 (2014)

[8] Jiang, M., Liang, W., Zhang, X.: Helicopter blades pyramid angle measurement based on panoramic vision technology. In: proceeding of the IEEE International Conference on Information and Automation 470-473 (2012)

[9] Lundstrom, T., Baqersad, J., Niezrecki, C.: Monitoring the dynamics of a helicopter main rotor with high-speed stereophotogrammetry. Exp. Techniques 40, 907–919 (2016)

[10] Endo, D.M.T., Montagnoli, A.N., Nicoletti, R.: Measurement of shaft orbits with photographic images and sub-sampling technique. Exp. Mech. 55, 471-481 (2015)

[11] Wu, R., Chen, Y., Pan, Y., Wang, Q., Zhang, D.: Determination of three-dimensional movement for rotary blades using digital image correlation. Opt. Lasers. Eng. 65, 38-45 (2015)

[12] Rizo-Patron, B.S., Sirohi, J.: Operational modal analysis of a helicopter rotor blade using digital image correlation. Exp. Mech. 57, 367-375 (2017)

[13] Wang, Y.Q., Sutton, M.A., Ke, X.D., Schreier, H.W., Reu, P.L., Miller, T.J.: On error assessment in stereo-based deformation measurements, part I: theoretical developments for quantitative estimates. Exp. Mech. 51, 405–422 (2011).

[14] Wu, R., Kong, C., Li, K., Zhang, D.: Real-time digital image correlation for dynamic strain measurement. Exp. Mech. 56, 833–843 (2016)

[15] Zappa, E., Hasheminejad, N.: Digital image correlation technique in dynamic applications on deformable targets. Exp. Techniques 41, 377–387 (2017)

[16] Barrows, D.A., Burner, A.W., Abrego, A.I., Olson, L.E.: Blade displacement measurements of the full-Scale UH-60A airloads rotor. In: 29th AIAA Applied Aerodynamics Conference (2011)

[17] Myers, G.C.: Flight measurements of helicopter blade motion with a comparison between theoretical and experimental results. National Advisory Committee for Aeronautics Technical Note No. 1266 (1947)

[18] Trainelli, L., Lovera, M., Rolando, A., Zappa, E., Gennaretti, M., Cordisco, P., et al.: Project MANOEUVRES – towards real-Time noise monitoring and enhanced rotorcraft handling based on rotor state measurements. In: 41st European Rotorcraft Forum (2015)

[19] Trainelli, L., Gennaretti, M., Zappa, E. et al.: Development and testing of innovative solutions for helicopter in-flight noise monitoring and enhanced control based on rotor state measurements. In: 42nd European Rotorcraft Forum (2016)

[20] Trainelli, L., Gennaretti, M., Bernardini, G. et al.: Innovative helicopter in-flight noise monitoring enabled by rotor state measurements. Noise Mapping 3, 190-215 (2016)

[21] Gennaretti, M., Bernardini, G., Serafini, J. et al.: Acoustic prediction of helicopter unsteady manoeuvres. In: 41st European Rotorcraft Forum (2015)

[22] Rolando, A., Rossi, F., Riboldi, C.E.D., et al.: The pilot acoustic indicator: a novel cockpit instrument for the greener helicopter pilot. In: 41st European Rotorcraft Forum (2015)

[23] Rolando, A., Rossi, F., Trainelli, L., Leonello, D., Maisano, G., Redaelli, M.: Demonstration and testing of the pilot acoustic indicator on a helicopter flight simulator. In: 42nd European Rotorcraft Forum (2016)

[24] Panza, S., Lovera, M.: Rotor state feedback in the design of rotorcraft attitude control laws, advances in aerospace guidance, navigation and control. Springer, New York (2015)

[25] Panza, S., Lovera, M., Bergamasco, M., Viganò, L.: Rotor state feedback in rotorcraft attitude control. In: 41st European Rotorcraft Forum (2015)

[26] McKillip, R.: A novel instrumentation system for measurement of helicopter rotor motions and loads data. In: American Helicopter Society 58th Annual Forum (2002)

[27] Colombo, A., Locatell,i A.: Measuring blade angular motions: a kinematical approach. In: 30th European Rotorcraft Forum (2004)

[28] Allred, C.J., Jolly, M.R., Buckner, G.D.: Real-time estimation of helicopter blade kinematics using integrated linear displacement sensors. Aerosp. Sci. Technol. 42, 274-286 (2015)

[29] Cigada, A., Colombo, A., Cordisco, P., et al.: Contactless rotor flapping sensor design, implementation and testing. In: American Helicopter Society 72nd Annual Forum (2016)

[30] Zappa, E., Trainelli, L., Cordisco, P. et al.: A novel contactless sensor for helicopter blade motion in-flight measurements. In: 42nd European Rotorcraft Forum (2016)

[31] Zappa, E., Liu, R., Trainelli, L., et al.: Laser and vision-based measurements of helicopter blade angles. Measurement 118, 29-42 (2018)

[32] Hartley, R.I., Sturm, P.: Triangulation. Comput Vis Image Und 68, 146-157 (1997)

[33] Zhang, Z.: Flexible camera calibration by viewing a plane from unknown orientations. In: proceedings of 7th IEEE International Conference on Computer Vision 666-673 (1999)

[34] Eggert, D.W., Lorusso, A., Fisher, R.B.: Estimating 3-D rigid body transformations: a comparison of four major algorithms. Mach. Vision Appl. 9, 272-290 (1997)

[35] C. Wöhler, 3D Computer Vision: Efficient Methods and Applications, Springer-Verlag Berlin Heidelberg 2009, DOI: 10.1007/978-3-642-01732-2_2

[36] Beau Tippetts, Dah Jye Lee, Kirt Lillywhite, James Archibald, Review of stereo vision algorithms and their suitability for resource-limited systems, Journal of Real-Time Image Processing, January 2016, Volume 11, Issue 1, pp 5–25

[37] Chaki, N., Shaikh, S.H., Saeed, K.: Exploring image binarization techniques. Springer, India (2014)

[38] Zhang, W., Li, W., Yan, J., Yu, L., Pan, C.: Adaptive threshold selection for background removal in fringe projection profilometry. Opt. Lasers Eng. 90, 209-216 (2017)

[39] Soille, P.: Morphological image analysis: principles and applications. Springer Science & Business Media (2013)

[40] Wang, Z.Z.: Automatic segmentation and classification of the reflected laser dots during analytic measurement of mirror surfaces. Opt. Lasers Eng. 83, 10-22 (2016)

[41] Ghiringhelli, G.L., Terraneo, M., Vigoni, E.: Improvement of structures vibroacoustics by widespread embodiment of viscoelastic materials. Aerosp. Sci. Technol. 28, 227-241 (2013)

[42] JCGM 100:2008 Evaluation of measurement data — Guide to the expression of uncertainty in measurement, https://www.bipm.org/en/publications/guides/gum.html

[43] Schank, T.C., Schulte, K.J.: A smart position sensor for articulated rotors. In: American Helicopter Society 71st Annual Forum (2015)

[44] Redaelli, M., Zappa, E., Liu, R., et al.: In-flight demonstration of a novel contactless sensor for helicopter blade motion measurement. In: 28th Annual Society of Flight Test Engineers European Chapter Symposium (2017)